Calibrating a long-term meteoric ^{10}Be delivery rate into eroding Western US glacial deposits by comparing meteoric and in situ-produced ^{10}Be depth profiles

Travis Clow[1], Jane K. Willenbring[1,2], Mirjam Schaller[3], Joel D. Blum[4], Christl, M.[5], Peter W. Kubik[5], Friedhelm von Blanckenburg[2]

[1]Department of Geological Sciences, Stanford University, Stanford, CA, USA
[2]GFZ German Research Centre for Geosciences, Earth Surface Geochemistry, Telegrafenberg, 14473 Potsdam, Germany
[3]Geodynamics, University of Tübingen, Wilhelmstraße 56, 72076 Tübingen, Germany
[4]Department of Earth and Environmental Sciences, University of Michigan, Ann Arbor, MI, USA
[5]ETH Zurich, Laboratory of Ion Beam Physics, HPK G23, Schafmattstrasse 20, ETH-Zurich, CH-8093 Zurich, Switzerland

Correspondence to: Travis Clow (tclow@stanford.edu)

Abstract. Meteoric ^{10}Be ($^{10}Be_{met}$) concentrations in soil profiles have great potential as a geochronometer and a tracer of Earth surface processes, particularly in fine-grained soils lacking quartz that would preclude the use of *in situ*-produced ^{10}Be ($^{10}Be_{in\ situ}$). One prerequisite for using this technique for accurately calculating rates and dates is constraining the delivery, or flux, of $^{10}Be_{met}$ to a site. However, few studies to date have quantified long-term (i.e. millennial) delivery rates, and none have determined a delivery rate for an eroding soil. In this study, we compared existing concentrations of $^{10}Be_{in\ situ}$ with new measurements of $^{10}Be_{met}$ in eroding soils sampled from the same depth profiles to calibrate a long-term $^{10}Be_{met}$ delivery rate. We did so on the Pinedale (~21-25 ky) and Bull Lake (~140 ky) glacial moraines at Fremont Lake, Wyoming (USA) where age, grain sizes, weathering indices, and soil properties are known, as are erosion/denudation rates calculated from $^{10}Be_{in\ situ}$. After ensuring sufficient beryllium retention in each profile, solving for the delivery rate of $^{10}Be_{met}$, and normalizing to the Holocene-average paleomagnetic intensity, we calculate $^{10}Be_{met}$ fluxes of 1.52 (+0.11/-0.21) x 10^6 atoms cm^{-2} y^{-1} and 1.31 (+0.43/-0.50) x 10^6 atoms cm^{-2} y^{-1} to the Pinedale and Bull Lake moraines, respectively, and compare these values to two widely-used $^{10}Be_{met}$ delivery rate estimation methods that substantially differ for this site. Accurately estimating $^{10}Be_{met}$ flux using these methods requires consideration of spatial scale as well as temporally varying parameters (i.e. paleomagnetic field intensity, solar modulation) to ensure the most realistic estimates of $^{10}Be_{met}$-derived erosion rates in future studies.

1 Introduction

^{10}Be is a cosmogenic isotope with a half-life of 1.39 +/- 0.01 My (Chmeleff et al., 2010) and its meteoric form ($^{10}Be_{met}$) is produced in the atmosphere through spallation reactions as high-energy cosmic rays collide with target nuclei (i.e. ^{14}N and ^{16}O) in the atmosphere (Lal and Peters, 1967). $^{10}Be_{met}$ is then delivered to Earth's surface via precipitation or as dry deposition at a flux of 0.1 – 2 x 10^6 atoms cm^{-2} y^{-1} followed by dissolved export in runoff, or depending on retentivity, adsorption onto fine-grained, reactive surfaces, typically clays and Fe- and Al-oxyhydroxides in soil horizons at the Earth's surface (Graly et al., 2010; Willenbring and von Blanckenburg, 2010). $^{10}Be_{met}$ has been used as a tracer of Earth surface processes, including estimating erosion rates at the soil-profile and river-catchment scales, soil residence times, ages of landforms over millennial to million-year timescales, and paleo-denudation rates from marine sedimentary records (Pavich et al., 1986; McKean et al., 1993; Jungers et al., 2009; Willenbring and von Blanckenburg, 2010; von Blanckenburg et al., 2012; von Blanckenburg and Bouchez, 2014; Wittman et al., 2015; von Blanckenburg et al., 2015; Portenga et al., 2019; Jelinski et al., 2019). Prerequisites for interpreting the concentrations and isotope ratios (i.e. $^{10}Be_{met}/^{9}Be$) as erosion or denudation (the sum of erosion and weathering) rates, respectively, include knowing the delivery rate of $^{10}Be_{met}$ (Pavich et al., 1986; Reusser et al., 2010; Graly et al, 2011; Heikkilä and von Blanckenburg, 2015; Dixon et al., 2018, Deng et al., 2020) and quantifying the mobility or retention of beryllium in soils (e.g. Bacon et al., 2012; Boschi and Willenbring, 2016a,b; Maher and von Blanckenburg, 2016; Dixon et al., 2018), not all of which was possible in many previous studies. The potential ability of using $^{10}Be_{met}$ depth profiles to obtain quantitative data on soil ages, residence times, production- and denudation rates in a similar manner as *in situ*-produced ^{10}Be ($^{10}Be_{in\ situ}$) depth profiles could prove to be highly advantageous, as it is easier to measure (due to much higher concentrations than $^{10}Be_{in\ situ}$) and can be employed in a much wider range of environments, as there is no dependence on the existence of coarse-grained quartz as is required for the analysis of $^{10}Be_{in\ situ}$.$^{10}Be_{in\ situ}$ shares a cosmic ray origin with $^{10}Be_{met}$ but differs in production method; $^{10}Be_{in\ situ}$ is produced within crystal lattices in surface rocks and soil, rather than in the atmosphere, with a well constrained total production rate of 4.01 atoms $g^{-1}y^{-1}$ at sea level, high latitude (Borchers et al., 2016), and is characterized by full retentivity and known production pathways with depth. $^{10}Be_{met}$, in stark contrast, is potentially subjected to variable adsorption depths, incomplete retentivity, and heterogeneous internal redistribution.

In this study, we compare the previously published $^{10}Be_{in\ situ}$ depth profiles of the Pinedale and Bull Lake terminal glacial moraines in Wind River, Wyoming (Schaller et al., 2009a,b) with new $^{10}Be_{met}$ concentrations from depth profiles from the same sample material to evaluate the long-term (i.e. millennial) delivery rate of $^{10}Be_{met}$ ($F_{(^{10}Be_{met})}$) to this site. This is the first study that evaluates $F_{(^{10}Be_{met})}$ for eroding soils as derived from the comparison of $^{10}Be_{in\ situ}$ and $^{10}Be_{met}$ depth profiles and erosion rates. We utilize previous knowledge of effective transient erosion rates from Schaller et al. (2009a), recalculated with revised parameters for *in situ* production of ^{10}Be, to constrain and locally calibrate $F_{(^{10}Be_{met})}$ to these moraines while considering the extent of $^{10}Be_{met}$ retention post-delivery. We then compare the resulting calculated $F_{(^{10}Be_{met})}$, with uncertainties determined via Monte Carlo simulations, with the predicted $F_{(^{10}Be_{met})}$ of Graly et al. (2011) and Heikkilä and von Blanckenburg (2015), normalizing each result for paleomagnetic field intensity variations over the Holocene. We also explore the practical differences between these flux estimates and advocate for each approach to be carried out when estimating $F_{(^{10}Be_{met})}$ for use in erosion rate calculations in future studies.

2 Background

2.1 Study Area

The Fremont Lake area of the Wind River Mountains (Wyoming, United States) experienced multiple glacial advances during the Pleistocene, evidenced by several moraines of Pinedale and Bull Lake age (Fig. 1; modified from original mapping and descriptions by Richmond, 1973). The climate is cold, semi-arid, and windy, with a 50-year precipitation rate and temperature of 27.6 cm y^{-1} and 2.1° C, respectively (WRCC, 2005), in the nearby town of Pinedale, Wyoming (~3.5 km southwest of the field area).

The Pinedale and Bull Lake age terminal moraines (hereafter referred to as Pinedale and Bull Lake moraines) analyzed in this study (Fig. 1) were formed by highland-to-valley mountain glaciers draining an ice cap accumulation zone that covered the mountain range. The Pinedale moraine is more steep-sided and boulder-strewn than the gently sloping Bull Lake

moraine, each with a total height of ~30 m (see Figs. 1b, 1c of Schaller et al., 2009a for detailed moraine transects). The pH of the moraine soils is well characterized; both profiles have pedogenic carbonate below 1 m, fixing the pH at depth to ~ 8 (Chadwick and Chorover, 2001). Hall and Shroba (1995) report pH data on profiles adjacent to those analyzed in this study, with average pH ranging from ~5.5 on the surface to ~8 at depth.

The depth profile samples analyzed for $^{10}Be_{met}$ reported here are the same sample material analyzed for $^{10}Be_{in\ situ}$ by Schaller et al. (2009a). We utilize bulk samples sieved to <2 mm for our analysis, extracted from the lower mineral soil developed on each moraine, both mixtures of reworked glacial till (composed of Archean granite, granodiorite, and dioritic gneiss) that have a high likelihood for inheritance from cosmic ray exposure prior to burial. The same reported depths and grain size distributions apply for each sample at depth. The primary mineral content in the deepest (unweathered, >2 mm size fraction) sample is (in order of decreasing abundance): plagioclase, quartz, biotite, K-feldspar, hornblende, and magnetite (Taylor and Blum, 1995). Secondary clay minerals in the 2 μm size fraction include kaolinite, vermiculite, illite, and smectite (Mahaney and Halvorson, 1986), with total clay content ranging from 3 to 10 wt% and 9 to 30 wt% for the Pinedale and Bull Lake profiles, respectively. Major element data is reported in Schaller et al. (2009b). Sr isotope measurements of the moraine soils and dust sources showed insignificant dust fluxes in the depth profiles of the Pinedale and Bull Lake moraines (Blum and Erel, 1997; Taylor and Blum, 1997).

2.2 Independent $^{10}Be_{met}$ Flux Estimation

Accurately estimating $F_{(^{10}Be_{met})}$ from field experiments is a topic of ongoing debate (e.g. Ouimet et al., 2015; Dixon et al., 2018), particularly in regard to the effect of precipitation rate on the flux (i.e. whether precipitation leads to additive or dilution effects on delivered $^{10}Be_{met}$, see *Willenbring and von Blanckenburg (2010)* and *Deng et al. (2020)* for extensive reviews). $F_{(^{10}Be_{met})}$ also varies through time, depending on solar and paleomagnetic field intensity, and has a spatial distribution primarily resulting from atmospheric mixing and scavenging. One means to estimate $^{10}Be_{met}$ production and delivery are $F_{(^{10}Be_{met})}$ estimates based on global atmospheric models (Field et al., 2006; Heikkilä and von Blanckenburg, 2015), which provide an estimate over large spatial scales. Another type of estimate is based on empirical, precipitation-

dependent field estimates of $^{10}Be_{met}$ inventories in dated soils (Graly et al., 2011) measured over annual time scales. The work of Ouimet et al. (2015) highlighted the necessity for local $F_{(^{10}Be_{met})}$ estimates that also integrate over millennial time scales against models such as these, as their comparison of $^{10}Be_{met}$ inventories and deposition rates from Pinedale- and Bull Lake-aged landforms in the Colorado Front Range showed that some were lower, and some exceeded, deposition rates from atmospheric models and precipitation collections.

The $F_{(^{10}Be_{met})}$ map of Heikkilä and von Blanckenburg (2015) utilizes the $^{10}Be_{met}$ production functions of Masarik and Beer (1999) combined with the ECHAM5 general circulation model (GCM). Production rates were scaled to reflect the solar modulation and magnetic field strength for the entire Holocene (280.94 MV) using measured ^{10}Be concentrations in ice cores. The authors ultimately present a global grid of predicted "pre-industrial" and "industrial" (referring to simulated aerosol and greenhouse gas concentrations) Holocene $F_{(^{10}Be_{met})}$ with an approximate cell size of 300 km x ~230 km. GCMs such as this are useful for modelling atmospheric mixing of $^{10}Be_{met}$, particularly in the stratosphere, as well as the regional effect of climate and its influence on $F_{(^{10}Be_{met})}$ via atmospheric circulation and precipitation (Heikkilä et al., 2012). At this latitude (~42.9° N), the pre-industrial predicted $F_{(^{10}Be_{met})}$ of 1.38 x 10^6 atoms cm^{-2} y^{-1} is nearly identical to that derived from the flux map of Field et al. (2006), which utilizes the GISS (Goddard Institute for Space Studies Model E) GCM to model production. While the pre-industrial modeled $F_{(^{10}Be_{met})}$ is more applicable for comparison for landforms of these ages, we utilize the industrial predicted $F_{(^{10}Be_{met})}$ of 2.37 x 10^6 atoms cm^{-2} y^{-1} as an upper bound uncertainty on their estimate.

On the other hand, the empirical, present-day estimates of $F_{(^{10}Be_{met})}$ from Graly et al. (2011) are based on measurements of $^{10}Be_{met}$ deposition rates from contemporary measurements of $^{10}Be_{met}$ in precipitation, corrected for dust and normalized to a modern (1951-2004) solar modulation value (700 MV). A first order estimate of the $F_{(^{10}Be_{met})}$ was empirically derived given latitude (L) and average precipitation rate (P) to the study area (Graly et al., 2011):

$$F(^{10}Be_{met}) = P \times (1.44 / (1 + EXP((30.7 - L) / 4.36)) + 0.63) \quad (1)$$

A predicted $F_{(^{10}Be_{met})}$ of 0.55 x 10^6 atoms cm^{-2} y^{-1} is calculated for these Wind River moraines using (Eq. 1), however in order to compare these two estimates with each other, as well as to our calculated $F_{(^{10}Be_{met})}$, we later normalize them all to a common paleomagnetic intensity datum (i.e. the Holocene).

3 Methods

3.1 Recalculating Previous Age Constraints

Ages for each moraine have been independently determined via multiple methods, with $^{10}Be_{in\ situ}$ surface exposure ages of boulders combined with $^{230}Th/U$ ages of nearby contemporaneous fluvial terraces yielding the most reliable average estimates of 21 ky and 140 ky for the Type-Pinedale and Bull Lake-age moraines, respectively (Gosse et al., 1995; Phillips et al., 1997; Easterbrook et al., 2003; Sharp et al., 2003). These ages closely correspond with global maximum ice volumes of marine oxygen isotope stages 2 and 6, respectively (Sharp et al., 2003). We recalculated the ^{10}Be boulder surface exposure ages used to constrain the timing of advancement of each moraine to its terminal position based on a recent revision of the ^{10}Be half-life, which affected the AMS standard values (Chmeleff et al., 2010), and the most recent nucleonic production rate of 3.92 atoms g^{-1} y^{-1} at sea level-high latitude (Borchers et al., 2016) (Table S1); the updated independent age constraints are 25 ky for the Pinedale moraine and remain at 140 ky for the Bull Lake moraine (see Supplementary Material for details).

3.2 Recalculating Previous Denudation Constraints

All moraine surfaces have been eroded to some extent after their deposition. To estimate the amount of erosion for our calculations, we utilize the previously reported denudation rates (comprising erosion and chemical loss by dissolution) for the Pinedale and Bull Lake moraines (Schaller et al., 2009a) from the same depth profiles and material analyzed in this study. The denudation rates of Schaller et al. (2009a) were calculated using a sea level, high latitude production rate of 5.1 atoms $g_{(qtz)}^{-1}$ y^{-1} (Stone, 2000) and a decay constant of 4.62 x 10^{-7} y^{-1}. Denudation rates were recalculated using CRONUS v.3 (Phillips et al., 2016) with the updated half-life and production rate values (Table S1) and updated independent age

constraints scaled to the sample altitude and latitude (Dunai, 2000) assuming two denudation rate scenarios: one of constant denudation since moraine deposition, and the other of transient denudation decreasing in magnitude since moraine deposition. Recalculated average denudation rates are 32.1 ± 2.7 mm ky^{-1} and 12.4 ± 4.8 mm ky^{-1} for the Pinedale and Bull Lake moraines, respectively, in the case of transient denudation, and are 15 mm ky^{-1} and 7.5 mm ky^{-1} for the Pinedale and Bull Lake moraines, respectively, in the case of constant denudation (Table 2). These recalculated denudation rates are determined from the best-fit Chi-Square solutions obtained from running Models 2, 4, 6, and 8 of Schaller et al. (2009a) with present-day parameters (See Supplementary Material for details). We consider the transient denudation rates to more closely approximate reality, as moraines, deposited as ~triangular landforms at the terminus of glaciers, initially experience faster denudation than that towards present day, where the moraines evolve to a concave-down parabolic geometry. As the curvature of the topography reduces over time, hillslope diffusion law dictates that the denudation rates will decrease as the moraine flattens.

To properly compare the transient denudation rates of Schaller et al. (2009a) with the $^{10}Be_{met}$–derived erosion rates using the methods of von Blanckenburg et al. (2012), the weathering component of denudation must be accounted for. For the Pinedale moraine, chemical weathering mass loss is estimated to be 16% of the denudation rate, while for the Bull Lake moraine, the chemical weathering mass loss accounts for 20% (Schaller et al., 2009b). If the weathering mass loss took place beneath the cosmic ray attenuation pathway, the recalculated average effective transient erosion rates are then 27.0 mm ky^{-1} and 9.9 mm ky^{-1} for the Pinedale and Bull Lake moraines, respectively. As there is no way to assess where this mass loss occurred, we instead utilize this degree of potential loss to place uncertainties (in addition to analytical uncertainties) on the effective transient erosion rates in all further calculations.

3.3 $^{10}Be_{met}$ Analysis

We analyzed approximately 1-2 g aliquots of the <2 mm grain-size moraine sediment fraction from the same ~10-15 cm depth intervals as Schaller et al. (2009a) analyzed for Be isotope abundance. We followed the sediment leaching procedure described in Ebert et al. (2012) and Wittmann et al. (2012), which was adapted from Bourlés (1988) and Guelke-Stelling and von Blanckenburg (2012), to extract Be isotopes from outer grain surfaces. Bulk samples underwent two steps to remove the

adsorbed beryllium: a 24-hr agitation in 0.5 M HCl (to extract amorphous oxide-bound Be), and 1 M hydroxylamine-hydrochloride (to remove crystalline-bound Be). After each step, the supernate was separated from the sediment.

To measure the adsorbed $^{10}Be_{met}$, the two aliquots of leached material were homogenized with ~200 µl of ^{9}Be carrier (Table 1) and 2 mL HF was added to the acid sample solution. This solution was nearly completely dried down and then dissolved in 1 additional mL of 50% HF acid and dried down completely, repeated once. We then added 10 mL ultrapure (18 MΩ) water to the warm fluoride residue and leached it for 1 h on a warm hotplate. The water containing the Be was gently removed via pipette and dried down separately. The Be in the water leach solution was extracted and purified by a form of the ion exchange chromatography procedure from von Blanckenburg et al. (2004) that was adapted for meteoric ^{10}Be purification by passing the leachate through anion (2 ml of BioRad 1x8 100-200 mesh resin) and cation (2x 1 ml BioRad AG50-X8 200-400 mesh) exchange resins, precipitated at pH ~9 using $NH_4OH:H_2O$ (1:1), washed twice with 2 ml ultrapure water with centrifugation in between, mixed with AgCl, centrifuged and dried overnight, and finally oxidized over open flame (>1000 °C; modified from Kohl & Nishiizumi, 1992). $^{10}Be_{met}/^{9}Be$ ratios were measured at the Zurich AMS Lab (Kubik and Christl, 2010) (S555 standard, nominal $^{10}Be/Be = 95.5 \times 10^{-12}$), from which the ^{10}Be concentration ($^{10}Be_{reac} = {}^{10}Be_{met}$) was calculated. Two carrier blanks analyzed with the samples register AMS $^{10}Be/^{9}Be$ ratios of $3.2 \pm 1.5\times10^{-15}$, and $2.2 \pm 1.5\times10^{-15}$ containing $\ll$0.1% of the ^{10}Be in analyzed samples.

3.4 $^{10}Be_{met}$ Flux Calculations

In an actively eroding setting, erosion rates can be calculated with knowledge of 1) the total inventory of $^{10}Be_{met}$ in the depth profile, 2) a known/estimated $^{10}Be_{met}$ flux to the location, 3) the $^{10}Be_{met}$ retention behavior, and 4) an assumption of approximate steady state conditions, which is only justified if the inventory of $^{10}Be_{met}$ is independent of the initial exposure age of the soil. Here, steady state means that $^{10}Be_{met}$ lost through erosion and decay equals the $^{10}Be_{met}$ gained from atmospheric flux (e.g. Brown et al., 1988; Willenbring and von Blanckenburg, 2010), a prerequisite of which is that the residence time of soil material containing meteoric ^{10}Be with respect to erosion is much less than the depositional age (Willenbring and von Blanckenburg, 2010). For an assumed steady state inventory, the inverse relationship between the local

erosion rate and the $^{10}Be_{met}$ content in the soil profile is exploited to determine a flux of $^{10}Be_{met}$ using the formulation of Brown (1987), rearranged as follows:

$$F(^{10}\mathrm{Be_{met}}) = E \times [^{10}\mathrm{Be}]_{\mathrm{reac}} + (I\lambda) \quad (2)$$

Where E is the erosion rate [g cm^{-2} y^{-1}], $F_{(^{10}Be_{met})}$ is the atmospheric flux of $^{10}Be_{met}$ [atoms cm^{-2} y^{-1}], I is the inheritance-corrected inventory of $^{10}Be_{met}$ [atoms cm^{-2}] in the depth profile, λ is the decay constant of ^{10}Be [y^{-1}], $[^{10}Be]_{reac}$ is the inheritance-corrected $^{10}Be_{met}$ concentration at the surface of the soil [atoms g^{-1}]. Inventories were calculated following Willenbring and von Blanckenburg (2010) using a depth-averaged regolith density (ρ) of 2.0 g cm^{-3} for each profile (Schaller et al., 2009a,b), where z is the depth to the bottom of the soil column and $[^{10}Be]_{reac}(z)$ is the concentration of $^{10}Be_{met}$ at depth, minus inheritance:

$$I = \int_0^z [^{10}\mathrm{Be}]_{\mathrm{reac}}(z)\rho dz \quad (3)$$

Both $^{10}Be_{met}$ and $^{10}Be_{in\ situ}$ depth profiles show indications of inherited nuclide concentrations at depth, likely due to incomplete glacial erosion resetting for each moraine (Schaller et al., 2009a). Higher concentrations at depth are observed for the Bull Lake moraine for both nuclide profiles (Fig. 1, Table 1), potentially due to the presence of pre-irradiated reworked till. We consider the lowest concentration observed for each depth profile as the inherited $^{10}Be_{met}$ concentration and subtract it from all measured concentrations.

Desorption of $^{10}Be_{met}$ can affect the inventory of $^{10}Be_{met}$ when erosion rates are low, water flux is high and soil chemistry favors mobility. Given that for these soil profiles pH ranges between 8 at depth and ~5.5 at the surface (Hall and Shroba, 1995), we must consider incomplete retention of beryllium and thus a reduced inventory and surface concentration used in (Eq. 2) (Bacon et al., 2012; Maher and von Blanckenburg, 2016). Applying a correction directly to the calculation of $^{10}Be_{met}$

flux is possible via a combination of (Eq. 2) (this study) and (Eq. 3) of von Blanckenburg et al. (2012), which requires an accurate estimation of the water flux out of the system (Q) and the Be partition coefficient (K_d).

$$F(^{10}Be_{met}) = (E \times [^{10}Be]_{reac} + (I\lambda)) + Q \times [^{10}Be]_{reac} \div K_d \quad (4)$$

K_d is estimated as 1 x 10^5 to 1 x 10^6 L kg^{-1} from the surficial pH of ~5.5 via Be sorption-desorption experiments from You et al. (1989). We estimate Q by proxy via the modern precipitation rate of 276 L m^{-2} y^{-1}.

Utilizing (Eq. 4) and previous knowledge of the effective transient erosion rates, we calculate the loss-corrected $F_{(^{10}Be_{met})}$ to the locations of these moraines. To further account for the full range of possible K_d values and transient erosion rates, we employ Monte Carlo simulations to determine the uncertainty of the calculated fluxes.

3.5 Monte Carlo Simulations

To assess the uncertainties of the calculated flux estimates, Monte Carlo simulations were used to solve for $F_{(^{10}Be_{met})}$ via (Eq. 4) over the entire range of possible values for each term (Table 3) for the Pinedale and Bull Lake moraines. This method is advantageous compared to traditional algebraic error propagation as it doesn't assume a Gaussian distribution, nor does it require an average K_d value input for each moraine, which is difficult to estimate accurately. We carry out each Monte Carlo simulation over 100,000 iterations and report uncertainties representing the 95% confidence intervals of each simulation. The MATLAB code used for these simulations is available in the Supplementary Material.

3.6 Normalizing flux estimates for geomagnetic intensity variations over the Holocene

Geomagnetic field strength has varied considerably from the late Pleistocene to present and exerts the primary quantifiable influence on temporal variability in the production rate of cosmogenic nuclides in an inverse fashion (Pigati and Lifton, 2004). Relative paleointensity over the last 140 ky is, on average, ~20-40% of the current geomagnetic intensity depending on the methodology employed (e.g. Frank et al., 1997; Valet et al., 2005). The flux map of Heikkilä and von Blanckenburg (2015) accounts for paleomagnetic variations over the Holocene via the reconstruction method of Steinhilber et al. (2012),

245 which effectively increases the production rate used in their model by 1.23 times the present-day rate by rescaling the modern solar modulation factor (Phi) and associated geomagnetic field intensity to that of the Holocene average (280.94 MV). As the estimations of flux from Graly et al. (2011) were normalized to reflect a solar modulation of 700 MV, we rescaled the modern Graly-derived $F_{(^{10}Be_{met})}$ to the average Holocene solar modulation factor of 280.94MV used in the flux map of Heikkilä and von Blanckenburg (2015) via Masarik and Beer (2009) and Steinhilber et al. (2012), following the
250 paleomagnetic and solar intensity normalization procedure of Deng et al. (2020).

To properly compare the model- and the precipitation-derived Holocene-average $F_{(^{10}Be_{met})}$ estimates with those calculated in this study, we must also normalize for geomagnetic and solar intensity variations for the Holocene. We rescaled our calculated loss-corrected $F_{(^{10}Be_{met})}$ for the Pinedale and Bull Lake moraines by first integrating the production rate relative to
255 the modern using the transport-corrected ^{10}Be marine core record of Christl et al. (2010) from 6 ky and 24 ky, respectively, and then normalizing these values over the Holocene, propagating the statistical uncertainties from the Monte Carlo simulations. These time intervals represent the calculated residence times of the soil profiles from the surface to the e-folding adsorption depth of $^{10}Be_{met}$ (20 and 30 cm for the Pinedale and Bull Lake moraines, respectively). This approach accounts for the cumulative effects of transient erosion and leaching by weighting geomagnetic intensity variations on $F_{(^{10}Be_{met})}$ towards
260 the present.

4 Results

4.1 Meteoric Cosmogenic ^{10}Be Concentrations

The measured $^{10}Be_{met}$ concentrations are reported along with the previously published $^{10}Be_{in\ situ}$ concentrations (Schaller et al., 2009a) for the Pinedale and Bull Lake profiles (Table 1); $^{10}Be_{met}$ depth profiles are presented for the Pinedale and Bull
265 Lake profiles in Figure 2. The Pinedale depth profile has $^{10}Be_{met}$ concentrations ranging from 3.57 (± 0.32) to 199.53 (± 5.26) x 10^6 atoms g^{-1}. The highest nuclide concentration is measured at 10 cm, rather than at the surface. Below this maximum value, concentrations decrease exponentially until reaching an asymptote at ~ 3 to 6 x 10^6 atoms g^{-1} from 43 cm to

the bottom of the profile (180 cm), the lowest of which we consider to be an inherited component. The Pinedale depth profile has an inventory of 6672 (± 122) x 10^6 atoms cm^{-2}.

The Bull Lake depth profile has $^{10}Be_{met}$ concentrations ranging from 6.32 (± 0.25) to 415.48 (± 12.46) x 10^6 atoms g^{-1}. The highest nuclide concentration is measured at the surface; below this, concentrations decrease in an approximately exponential fashion until the reaching an asymptote at ~ 6 to 8 x 10^6 atoms g^{-1} from 64 cm to the bottom of the profile (130 cm), the lowest of which we also consider to be an inherited component. The Bull Lake depth profile has an inventory of 19021 (± 318) x 10^6 atoms cm^{-2}. The $^{10}Be_{met}$ inventory from the Bull Lake moraine is roughly 3 times higher than that of the Pinedale moraine.

4.2 $^{10}Be_{met}$ Fluxes

The loss-corrected $F_{(^{10}Be_{met})}$ as calculated from (Eq. 4) is 1.08 (+0.10/-0.16) x 10^6 atoms cm^{-2} y^{-1} and 1.05 (+0.35/-0.40) x 10^6 atoms cm^{-2} y^{-1} for the Pinedale and Bull Lake moraines, respectively (Table 3), where the Monte Carlo-derived uncertainties reflect the 95% confidence interval of all possible input parameters.

Retention calculations from (Eq. 4) and the Monte Carlo simulation indicate that the potential desorption loss at the surface of the Pinedale and Bull Lake profiles ranges from 0.4% to 4.9% and 0.8% to 15.4%, respectively.

These loss-corrected calculated fluxes are then normalized for paleomagnetic field intensity variations over the Holocene and compared in order to evaluate the $F_{(^{10}Be_{met})}$ to this area. The Holocene-average loss-corrected $F_{(^{10}Be_{met})}$ from this study are 1.52 (+0.11/-0.21) x 10^6 atoms cm^{-2} y^{-1} and 1.31 (+0.43/-0.50) x 10^6 atoms cm^{-2} y^{-1} for the Pinedale and Bull Lake moraines, respectively (Table 3).

The predicted Holocene-average $F_{(^{10}Be_{met})}$ of Graly et al. (2011) for this site is 0.83 x 10^6 atoms cm^{-2} y^{-1} (Table 3). As the pre-Industrial flux map of Heikkilä and von Blanckenburg (2015) already presents a Holocene-average $F_{(^{10}Be_{met})}$ of 1.38 x 10^6 atoms cm^{-2} y^{-1}, no normalization for this method needs to be carried out.

5 Discussion

5.1 Cosmogenic Nuclide Profiles

An approximately exponential decrease in $^{10}Be_{met}$ with depth is observed for the Pinedale and Bull Lake moraines (Fig. 2). This trend can be explained most simply by the reactive transport of dissolved $^{10}Be_{met}$ with infiltrating water (e.g. Willenbring and von Blanckenburg, 2010), as exponential $^{10}Be_{met}$ profiles are predicted by reactive transport models (Maher and von Blanckenburg, 2016).

The maximum $^{10}Be_{met}$ concentration for the Pinedale moraine is measured at 10 cm depth, rather than the most surficial sample (3 cm). This peak concentration corresponds with the clay rich layer of the B-horizon in the soil profile (Table 1). This potentially indicates that this layer acts as a zone of illuviation, often observed in soil profiles that contain a mid-depth clay-rich horizon (e.g. Monaghan et al., 1992) formed by vertical transport of soil particles containing $^{10}Be_{met}$ (Jagercikova et al., 2016). This subsurface maximum could be the result of smaller grain sizes within this horizon, as these grains have a higher surface area per unit mass and can exchange ions more easily (Brown et al., 1992; Willenbring and von Blanckenburg, 2010). Alternatively, enhanced $^{10}Be_{met}$ incorporation into the lattices of newly formed clays and oxyhydroxides at depth (e.g. Barg et al., 1997) might explain this maximum. This phenomenon is not observed for the Bull Lake moraine; the highest clay content observed in the profile is in the Bk-horizon at a depth of 43 cm (Schaller et al., 2009a,b), however no increase or anomalous high $^{10}Be_{met}$ concentration is observed (Fig. 2, Table 1).

Peculiarly, the observed mixing depths for the Pinedale and Bull Lake moraines as determined from the $^{10}Be_{in\ situ}$ depth profiles of Schaller et al. (2009a) (~40 and 50 cm, respectively) are not observed for the $^{10}Be_{met}$ depth profiles (Fig. 2). A couple of viable reasons for a lack of a mixing signal in the $^{10}Be_{met}$ depth profiles exist. The different grain sizes analyzed

here and in Schaller et al. (2009a) might exhibit different diffusion coefficients, however an observable trend in grain size with depth within the $^{10}Be_{in\ situ}$ mixing layer would likely be observed if this were the case. Another possibility is that the advection of $^{10}Be_{met}$ from the surface swamps the effect of mixing that is apparent in the $^{10}Be_{in\ situ}$ depth profiles. This could indicate that continual $^{10}Be_{met}$ delivery and reactive flow resets the $^{10}Be_{met}$ profile at timescales much shorter than that of physical mixing. Profiles with a relatively low surficial pH (<5) might be particularly susceptible to this phenomenon due to incomplete retention or differential mobility of $^{10}Be_{met}$ (Kaste and Baskaran, 2011), although the profiles analyzed here are not likely to show appreciable (>15%) $^{10}Be_{met}$ loss at depth due to retention issues. Nonetheless, the formation of a clay horizon in the Pinedale moraine may indicate that soil horizonation happens more rapidly than soil mixing, as inferred from the $^{10}Be_{in\ situ}$ depth profile (Schaller et al., 2009a), suggesting that $^{10}Be_{met}$ advection from the surface is a more likely explanation.

5.1.1 $^{10}Be_{met}$ Retention

A range of possibilities exist for retention effects and associated surficial $^{10}Be_{met}$ loss for these profiles. For the highest Kd estimate, at 1 x 10^6 L kg^{-1}, potential loss is as low as 0.4% and 0.8% for the Pinedale and Bull Lake profiles, respectively. On the other hand, for the lowest Kd estimate, at 1 x 10^5 L kg^{-1}, $^{10}Be_{met}$ loss due to desorption could be as great as 4.9% and 15.4% at the surface of the Pinedale and Bull Lake profiles, respectively. Despite this, the Monte Carlo simulations indicate a low probability for loss to this degree, particularly for the Pinedale profile, as evidenced by the relatively shallow tail for each histogram (Fig. S1), with $F_{(^{10}Be_{met})}$ results within the 95% confidence interval. While the possibility of desorption cannot be ruled out, we note that $^{10}Be_{met}$ mobilization to depth does not have an appreciable effect on $F_{(^{10}Be_{met})}$ in the vast majority of simulations. Even in the worst-case scenario, the magnitude of the potential loss does not substantially affect our calculated $F_{(^{10}Be_{met})}$ estimates within uncertainties.

5.2 $^{10}Be_{met}$ flux estimation; sources of variability

The calculated, loss- and paleointensity-corrected $F_{(^{10}Be_{met})}$ of 1.52 (+0.11/-0.21) x 10^6 atoms cm^{-2} y^{-1} and 1.31 (+0.43/-0.50) x 10^6 atoms cm^{-2} y^{-1} for the Pinedale and Bull Lake moraines, respectively, are higher compared to that estimated by Graly et

al. (2011), at 0.83 x 10^6 atoms cm^{-2} y^{-1}, and agree within uncertainty with that predicted by Heikkilä and von Blanckenburg (2015), at 1.38 x 10^6 atoms cm^{-2} y^{-1} (Table 3). The considerable discrepancy between the predicted $F_{(^{10}Be_{met})}$ of each method arises primarily from differences in how each methodology treats the influence that precipitation rate has on the flux to a given area and, in particular for this study, how large of an area is covered. The 310 km x 228 km flux map grid cell of Heikkilä and von Blanckenburg (2015) covers the entirety of the Wind River Range and the surrounding, relatively low-lying flatlands (Fig. 1), where precipitation estimates vary considerably, by over an order of magnitude (WRCC, 2005), due to elevation and topographic effects on precipitation (Hostetler and Clark, 1997). For example, if one were to estimate $F_{(^{10}Be_{met})}$ from Graly et al. (2011) via (Eq. 1) to nearby Fish Lake Mountain contained within the same grid cell, with a modern precipitation rate of 128 cm y^{-1} (WRCC, 2005), the $F_{(^{10}Be_{met})}$ would be 2.5 x 10^6 atoms cm^{-2} y^{-1}, substantially higher than that predicted from Heikkilä and von Blanckenburg (2015). Considering this alone, it is not surprising that such a discrepancy exists between methods, nor is this a unique occurrence (e.g. Jungers et al., 2009; Schoonejans et al., 2017; Dixon et al., 2018; Deng et al., 2020).

Each approach has its own set of shortcomings, precluding agreement between each approach in sites such as this. The flux map of Heikkilä and von Blanckenburg (2015) has a coarse resolution and does not handle short wavelength orographic effects well, along with being model based and requiring many assumptions on atmospheric scavenging. The formula of Graly et al. (2011), on the other hand, does not take atmospheric circulation into account, instead relying on data from sites with relatively high rates of precipitation to derive an empirical formula. Recent work by Deng et al. (2020) highlights the potential for precipitation estimates to differ from GCM-derived estimates due to short timescale additive effects (*sensu* Willenbring and von Blanckenburg, 2010). Further, they find that in the majority of studies globally, GCM- and soil-derived $F_{(^{10}Be_{met})}$ estimates agree within a factor of two. That the calculated fluxes of this study agree with the GCM-modelled pre-Industrial $F_{(^{10}Be_{met})}$ of Heikkilä and von Blanckenburg (2015) provides further evidence of this general observation. In any event, the strength of future $^{10}Be_{met}$ studies relies upon careful consideration of beryllium retention, spatial scale, and paleomagnetic intensity when determining $F_{(^{10}Be_{met})}$. As calculating a long-term delivery rate of $F_{(^{10}Be_{met})}$ for a particular site

using $^{10}Be_{in\text{-}situ}$ and $^{10}Be_{met}$ is both costly and time-intensive, it is especially prudent to estimate $F_{(^{10}Be_{met})}$ using both methods compared here for robust $^{10}Be_{met}$ erosion rate calculations in the future.

6. Conclusions

In this study, we compare new meteoric ^{10}Be and previously published *in situ*-produced ^{10}Be depth profile measurements from the well-characterized Pinedale (~21-25 ky) and Bull Lake (~140 ky) moraines of Wind River, Wyoming. Our ability to utilize previous knowledge of transient erosion rates from the $^{10}Be_{in\ situ}$ depth profile measurements of Schaller et al. (2009a), recalculated with revised parameters, allows us to calculate loss-corrected Holocene average $^{10}Be_{met}$ fluxes of 1.52 (+0.11/-0.21) x 10^6 atoms cm^{-2} y^{-1} and 1.31 (+0.43/-0.50) x 10^6 atoms cm^{-2} y^{-1} to the Pinedale and Bull Lake moraines, respectively. Comparing these fluxes to two widely-used independent estimation methods reveals that the empirical flux estimate of Graly et al. (2011), after normalizing for Holocene paleomagnetic intensity, at 0.83 x 10^6 atoms cm^{-2} y^{-1}, is lower than the calculated fluxes, and the modeled Holocene flux estimate of Heikkila and von Blanckenburg (2015), at 1.38 x 10^6 atoms cm^{-2} y^{-1}, agrees within uncertainty to the calculated fluxes. We find that loss of $^{10}Be_{met}$ in these profiles due to pH-influenced mobility/dissolution effects exerts a relatively minor potential control (biasing from 1% up to 15%) on flux calculations. Inspection of the $^{10}Be_{met}$ depth profiles and their near-surface concentrations suggest that soil mixing to depths of 40 and 50 cm, as observed for the Pinedale and Bull Lake $^{10}Be_{in\ situ}$ depth profiles, respectively, is not represented by the finer grain sizes analyzed in this study. The lack of a mixing signal may be most simply explained by a swamping effect from continual delivery and advection of $^{10}Be_{met}$ from the surface that occurs over more rapid timescales than soil mixing. These differences in the depth-concentration relationships between $^{10}Be_{met}$ and $^{10}Be_{in\ situ}$ might open up a new area of research to study particle movement in soils.

Author Contribution

TC is a current Ph.D. student at Stanford University and conducted the majority of the work during 2018-2019 under the supervision of JWK, who contributed to several drafts of the original manuscript as well as preparation of the meteoric data set. MS and JDB contributed via ^{10}Be data acquisition, interpretation, and discussion; MC and PWK contributed via AMS

measurements at ETH-Zurich. FvB assisted in interpretation of the comparative data set and associated discussion of meteoric ^{10}Be flux estimates, mobility/retention, and paleomagnetic field intensity normalization.

Competing Interests

The authors declare no competing interests for this manuscript.

Acknowledgement

This work was made possible through the German Science Foundation Grant *BL562/7* and an Alexander von Humboldt Postdoctoral Fellowship. Support for TC came from a Career grant to Willenbring from NSF #1651243. The authors thank three anonymous reviewers for constructive comments and suggestions which greatly improved the manuscript.

References

Bacon, A. R., Richter, D. D., Bierman, P. R., and Rood, D. H.: Coupling meteoric 10Be with pedogenic losses of 9Be to improve soil residence time estimates on an ancient North American interfluve, Geology, 40(9), 847-850, https://doi.org/10.1130/G33449.1, 2012

Barg, E., Lal, D., Pavich, M. J., Caffee, M. W., and Southon, J. R.: Beryllium geochemistry in soils; evaluation of 10Be/ 9Be ratios in authigenic minerals as a basis for age models. Chemical Geology, 140, 237-258, https://doi.org/10.1016/S0009-2541(97)00051-X, 1997.

Blum, J. D., and Erel, Y.: Rb/Sr isotope systematics of a granitic soil chronosequence: The importance of biotite weathering, Geochimica et Cosmochimica Acta, 61(15), 3193-3204, https://doi.org/10.1016/S0016-7037(97)00148-8, 1997.

Borchers, B., Marrero, S., Balco, G., Caffee, M., Goehring, B., Lifton, N., ... and Stone, J.: Geological calibration of spallation production rates in the CRONUS-Earth project, Quaternary Geochronology, 31, 188-198, https://doi.org/10.1016/j.quageo.2015.01.009, 2016.

Bourlès, D.: Étude de la géochimie de l'isotope cosmogénique ^{10}Be et de son isotope stable 9Be en milieu océanique: application à la datation des sédiments marins, Ph.D. thesis, Université Paris XI, Centre d'Orsay, 1988.

Boschi, V., Willenbring, J.K.:The role of pH, organic matter composition and mineralogy on the sorption behavior of beryllium. Environmental Chemistry. http://dx.doi.org/10.1071/EN15107, 2016a.

Boschi, V., Willenbring, J.K.: Beryllium Desorption from Minerals and Organic Ligands Over Time. Chemical Geology, 439(7) 52–58. http://dx.doi.org/10.1016/j.chemgeo.2016.06.009, 2016b.

Brown, L.: 10Be as a tracer of erosion and sediment transport. Chemical Geology: Isotope Geoscience section, 65(3-4), 189-196, https://doi.org/10.1016/0168-9622(87)90002-9, 1987.

Brown, L., Pavich, M. J., Hickman, R. E., Klein, J., Middleton, R.: Erosion of the Eastern United States observed with 10Be. Earth Surface Processes and Landforms, 13, 441-457, https://doi.org/10.1002/esp.3290130509, 1988.

Brown, E. T., Edmond, J. M., Raisbeck, G. M., Bourlès, D. L., Yiou, F., and Measures, C. I.: Beryllium isotope geochemistry in tropical river basins, Geochimica et Cosmochimica Acta, 56(4), 1607-1624, https://doi.org/10.1016/0016-7037(92)90228-B, 1992.

Chadwick, O. A., & Chorover, J., The chemistry of pedogenic thresholds, Geoderma, 100(3-4), 321-353, https://doi.org/10.1016/S0016-7061(01)00027-1, 2001.

Chmeleff, J., von Blanckenburg, F., Kosser, K., and Jakob, D.: Determination of the 10Be half-life by multicollecter ICP-MS and liquid scintillation counting, Nuclear Instruments and Methods in Physics Research Section B: Beam Interactions with Materials and Atoms, 268(2), 192–199, https://doi.org/10.1016/j.nimb.2009.09.012, 2010.

Christl, M., Lippold, J., Steinhilber, F., Bernsdorff, F., and Mangini, A.: Reconstruction of global 10Be production over the past 250 ka from highly accumulating Atlantic drift sediments, Quaternary Science Reviews, 29(19-20), 2663-2672, https://doi.org/10.1016/j.quascirev.2010.06.017, 2010.

Deng, K., Wittmann, H., and von Blanckenburg, F.: The depositional flux of meteoric cosmogenic 10Be from modelling and observation, Earth and Planetary Science Letters, 550, 116530, https://doi.org/10.1016/j.epsl.2020.116530, 2020.

Dixon, J. L., Chadwick, O. A., and Pavich, M. J.: Climatically controlled delivery and retention of meteoric 10Be in soils, Geology, 46(10), 899-902, https://doi.org/10.1130/G45176.1, 2018.

Dunai, T. J.: Scaling factors for production rates of in situ produced cosmogenic nuclides: a critical reevaluation, Earth and Planetary Science Letters, 176(1), 157-169, https://doi.org/10.1016/S0012-821X(99)00310-6, 2000.

Easterbrook, D. J., Pierce, K., Gosse, J., Gillespie, A., Evenson, E., and Hamblin, K.: Quaternary geology of the western United States, in: Quaternary Geology of the United States, edited by: Easterbrook, D. J., Desert Res. Inst., Reno, Nev., 19-79, 2003.

Ebert, K., Willenbring, J., Norton, K. P., Hall, A., and Hättestrand, C.: Meteoric 10Be concentrations from saprolite and till in northern Sweden: Implications for glacial erosion and age, Quaternary Geochronology, 12, 11-22, https://doi.org/10.1016/j.quageo.2012.05.005, 2012.

Field, C. V., Schmidt, G. A., Koch, D., and Salyk, C.: Modeling production and climate-related impacts on 10Be concentration in ice cores, Journal of Geophysical Research: Atmospheres, 111(D15), https://doi.org/10.1029/2005JD006410, 2006.

Frank, M., Schwarz, B., Baumann, S., Kubik, P. W., Suter, M., and Mangini, A.: A 200 kyr record of cosmogenic radionuclide production rate and geomagnetic field intensity from 10Be in globally stacked deep-sea sediments, Earth and Planetary Science Letters, 149(1-4), 121-129, https://doi.org/10.1016/S0012-821X(97)00070-8, 1997.

Guelke-Stelling, M., and von Blanckenburg, F.: Fe isotope fractionation caused by translocation of iron during growth of bean and oat as models of strategy I and II plants, Plant and soil, 352(1-2), 217-231, https://doi.org/10.1007/s11104-011-0990-9, 2012.

Gosse, J. C., Klein, J., Lawn, B., Middleton, R., and Evenson, E. B.: Beryllium-10 dating of the duration and retreat of the last Pinedale glacial sequence, Science, 268(5215), 1329-1333, https://doi.org/10.1126/science.268.5215.1329, 1995.

Graly, J. A., Bierman, P. R., Reusser, L. J., and Pavich, M. J.: Meteoric ^{10}Be in soil profiles—a global meta-analysis, Geochimica et Cosmochimica Acta, 74(23), 6814-6892, https://doi.org/10.1016/j.gca.2010.08.036, 2010.

Graly, J. A., Reusser, L. J., and Bierman, P. R.: Short and long-term delivery rates of meteoric 10Be to terrestrial soils, Earth and Planetary Science Letters, 302(3-4), 329-336, https://doi.org/10.1016/j.epsl.2010.12.020, 2011.

Hall, R. D., and Shroba, R. R.: Soil evidence for a glaciation intermediate between the Bull Lake and Pinedale glaciations at Fremont Lake, Wind River Range, Wyoming, USA, Arctic and Alpine Research, 27(1), 89-98, https://doi.org/10.2307/1552071, 1995.

Heikkilä, U. and Smith, A. M.: Influence of model resolution on the atmospheric transport of 10Be, Atmospheric Chemistry and Physics, 12(21), 10601-10612, https://doi.org/10.5194/acp-12-10601-2012, 2012.

Heikkilä, U. and Von Blanckenburg, F.: The global distribution of Holocene meteoric 10Be fluxes from atmospheric models, GFZ Data Services, GFZ Potsdam, Germany, http://doi.org/10.5880/GFZ.3.4.2015.001, 2015.

Hostetler, S. W., and Clark, P. U.: Climatic controls of western US glaciers at the last glacial maximum, Quaternary Science Reviews, 16(6), 505-511, https://doi.org/10.1016/S0277-3791(96)00116-3, 1997.

Jagercikova, M., Cornu, S., Bourlès, D., Evrard, O., Hatté, C. and Balesdent, J.: Quantification of vertical solid matter transfers in soils during pedogenesis by a multi-tracer approach, Journal of Soils and Sediments, 17, 408-422, https://doi.org/10.1007/s11368-016-1560-9, 2016.

Jelinski, N., Willenbring, J.K., Schumacher, T.E., Li, S. Lobb, D.A., Papiernik, S.K., and Yoo, K.: Meteoric Beryllium-10 as a tracer of cumulative erosion due to post-settlement land use in west-central Minnesota, USA, Journal of Geophysical Research – Earth Surface, 124(4), 874-901, https://doi.org/10.1029/2018JF004720, 2019.

Jungers, M. C., Bierman, P. R., Matmon, A., Nichols, K., Larsen, J., and Finkel, R.: Tracing hillslope sediment production and transport with in situ and meteoric 10Be, Journal of Geophysical Research: Earth Surface, 114(F4), https://doi.org/10.1029/2008JF001086, 2009.

Kaste, J. M., and Baskaran, M.: Meteoric 7Be and 10Be as process tracers in the environment, in: Handbook of environmental isotope geochemistry, edited by: Baskaran, M., Springer, Berlin, Heidelberg, 61-85, https://doi.org/10.1007/978-3-642-10637-8_5, 2012.

Kubik, P. W., and Christl, M.: 10Be and 26Al measurements at the Zurich 6 MV Tandem AMS facility, Nuclear Instruments and Methods in Physics Research Section B: Beam Interactions with Materials and Atoms, 268(7-8), 880-883, https://doi.org/10.1016/j.nimb.2009.10.054, 2010.

Kohl, C. P., and Nishiizumi, K.: Chemical isolation of quartz for measurement of in-situ -produced cosmogenic nuclides, Geochimica et Cosmochimica Acta, 56(9), 3583-3587, https://doi.org/10.1016/0016-7037(92)90401-4, 1992.

Lal, D. and Peters, B.: Cosmic ray produced radioactivity on the Earth, in: Kosmische Strahlung II/Cosmic Rays II, edited by: Sitte, K., Springer, Berlin, Heidelberg, 551-612, https://doi.org/10.1007/978-3-642-46079-1_7, 1967.

Mahaney, W. C., and Halvorson, D. L.: Rates of mineral weathering in the Wind River Mountains, western Wyoming, in: Rates of chemical weathering of rocks and minerals, edited by: Colman, S., and Dethier, D., Academic Press, Cambridge, Massachusetts, 147-167, 1986.

Maher, K., and von Blanckenburg, F.: Surface ages and weathering rates from 10Be (meteoric) and 10Be/9 Be: insights from differential mass balance and reactive transport modeling, Chemical Geology, 446, 70-86, https://doi.org/10.1016/j.chemgeo.2016.07.016, 2016.

Masarik, J., and Beer, J.: Simulation of particle fluxes and cosmogenic nuclide production in the Earth's atmosphere, Journal of Geophysical Research: Atmospheres, 104(D10), 12099-12111, https://doi.org/10.1029/1998JD200091, 1999.

Masarik, J., and Beer, J.: An updated simulation of particle fluxes and cosmogenic nuclide production in the Earth's atmosphere, Journal of Geophysical Research: Atmospheres, 114(D11), https://doi.org/10.1029/2008JD010557, 2009.

Mckean, J.A., Dietrich, W.E., Finkel, R.C., Southon, J.R., and Caffee, M.W.: Quantification of Soil Production and Downslope Creep Rates from Cosmogenic Be-10 Accumulations on a Hillslope Profile, Geology, 21, 343-346, https://doi.org/10.1130/0091-7613(1993)021<0343:QOSPAD>2.3.CO;2, 1993.

Monaghan, M. C., McKean, J., Dietrich, W., and Klein, J.: 10Be chronometry of bedrock-to-soil conversion rates, Earth and Planetary Science Letters, 111(2-4), 483-492, https://doi.org/10.1016/0012-821X(92)90198-5, 1992.

Ouimet, W., Dethier, D., Bierman, P., Wyshnytzkyr, C., Shea, N., and Rood, D. H.: Spatial and temporal variations in meteoric 10Be inventories and long-term deposition rates, Colorado Front Range, Quaternary Science Reviews, 109, 1-12, https://doi.org/10.1016/j.catena.2014.12.008, 2015.

Pavich, M. J., Brown, L., Harden, J., Klein, J., and Middleton, R.: 10Be distribution in soils from Merced River terraces, California, Geochimica et Cosmochimica Acta, 50(8), 1727-1735, https://doi.org/10.1016/0016-7037(86)90134-1, 1986.

Phillips, F. M., Zreda, M. G., Gosse, J. C., Klein, J., Evenson, E. B., Hall, R. D., Chadwick, O.A., and Sharma, P.: Cosmogenic 36Cl and 10Be ages of Quaternary glacial and fluvial deposits of the Wind River Range, Wyoming, Geological Society of America Bulletin, 109(11), 1453-1463, https://doi.org/10.1130/0016-7606(1997)109<1453:CCABAO>2.3.CO;2, 1997.

Phillips, F. M., Argento, D. C., Balco, G., Caffee, M. W., Clem, J., Dunai, T. J., ... and Jull, A. T.: The CRONUS-Earth project: a synthesis, Quaternary Geochronology, 31, 119-154, https://doi.org/10.1016/j.quageo.2015.09.006, 2016.

Pigati, J. S. and Lifton, N. A.: Geomagnetic effects on time-integrated cosmogenic nuclide production with emphasis on in situ 14C and 10Be, Earth and Planetary Science Letters, 226(1-2), 193-205, https://doi.org/10.1016/j.epsl.2004.07.031, 2004.

Portenga, E.W., Bierman, P.R., Trodick Jr, C.D., Greene, S.E., DeJong, B.D., Rood, D.H., and Pavich, M.J.: Erosion rates and sediment flux within the Potomac River basin quantified over millennial timescales using beryllium isotopes, GSA Bulletin, 131(7-8), 1295-1311, https://doi.org/10.1130/B31840.1, 2019.

Reusser, L., Graly, J., Bierman, P., and Rood, D.: Calibrating a long-term meteoric 10Be accumulation rate in soil, Geophysical Research Letters, 37(19), https://doi.org/10.1029/2010GL044751, 2010.

Richmond, G. M.: Geologic map of the Fremont Lake south quadrangle, Sublette County, Wyoming, Map 1138, https://doi.org/10.3133/gq1138, 1973.

Schaller, M., Ehlers, T. A., Blum, J. D., and Kyrllenberg, M. A.: Quantifying glacial moraine age, denudation, and soil mixing with cosmogenic nuclide depth profiles, Journal of Geophysical Research: Earth Surface, 114(F1), https://doi.org/10.1029/2007JF000921, 2009a.

Schaller, M., Blum, J. D., & Ehlers, T. A.: Combining cosmogenic nuclides and major elements from moraine soil profiles to improve weathering rate estimates, Geomorphology, 106(3-4), 198-205, https://doi.org/10.1016/j.geomorph.2008.10.014, 2009b.

Schoonejans, J., Vanacker, V., Opfergelt, S., and Christl, M.: Long-term soil erosion derived from in-situ 10Be and inventories of meteoric 10Be in deeply weathered soils in southern Brazil. Chemical Geology, 466, 380-388, https://doi.org/10.1016/j.chemgeo.2017.06.025, 2017.

Sharp, W. D., Ludwig, K. R., Chadwick, O. A., Amundson, R., and Glaser, L. L.: Dating fluvial terraces by 230 Th/U on pedogenic carbonate, Wind River Basin, Wyoming, Quaternary Research, 59(2), 139-150, https://doi.org/10.1016/S0033-5894(03)00003-6, 2003.

Steinhilber, F., Abreu, J. A., Beer, J., and McCracken, K. G.: Interplanetary magnetic field during the past 9300 years inferred from cosmogenic radionuclides, Journal of Geophysical Research: Space Physics, 115(A1), https://doi.org/10.1029/2009JA014193, 2010.

Stone, J. O.: Air pressure and cosmogenic isotope production, Journal of Geophysical Research: Solid Earth, 105(B10), 23753-23759, https://doi.org/10.1029/2000JB900181, 2000.

Taylor, A. and Blum, J. D.: Relation between soil age and silicate weathering rates determined from the chemical evolution of a glacial chronosequence, Geology, 23(11), 979-982, https://doi.org/10.1130/0091-7613(1995)023<0979:RBSAAS>2.3.CO;2, 1995.

Taylor, A. and Blum, J. D.: Relation between soil age and silicate weathering rates determined from the chemical evolution of a glacial chronosequence: Reply, Geology, 25(4), 382-383, 1997.

Valet, J. P., Meynadier, L., and Guyodo, Y.: Geomagnetic dipole strength and reversal rate over the past two million years, Nature, 435(7043), 802-805, https://doi.org/10.1038/nature03674, 2005.

von Blanckenburg, F., Hewawasam, T., and Kubik, P. W.: Cosmogenic nuclide evidence for low weathering and denudation in the wet, tropical highlands of Sri Lanka, Journal of Geophysical Research: Earth Surface, 109(F3), https://doi.org/10.1029/2003JF000049, 2004.

von Blanckenburg, F., Bouchez, J., and Wittmann, H.: Earth surface erosion and weathering from the 10Be (meteoric)/9Be ratio, Earth and Planetary Science Letters, 351, 295-305, https://doi.org/10.1016/j.epsl.2012.07.022, 2012.

von Blanckenburg, F., and Bouchez, J.: River fluxes to the sea from the ocean's 10Be/9Be ratio. Earth and Planetary Science Letters, 387, 34-43, https://doi.org/10.1016/j.epsl.2013.11.004, 2014.

von Blanckenburg, F., Bouchez, J., Ibarra, D.E., and Maher, K.: Stable runoff and weathering fluxes into the oceans over Quaternary climate cycles, Nature Geoscience, 8, 538-U146, https://doi.org/10.1038/ngeo2452, 2015.

Willenbring, J. K., and von Blanckenburg, F.: Meteoric cosmogenic Beryllium-10 adsorbed to river sediment and soil: Applications for Earth-surface dynamics. Earth-Science Reviews, 98(1-2), 105-122, https://doi.org/10.1016/j.earscirev.2009.10.008, 2010.

Wittmann, H., Von Blanckenburg, F., Bouchez, J., Dannhaus, N., Naumann, R., Christl, M., and Gaillardet, J.: The dependence of meteoric 10Be concentrations on particle size in Amazon River bed sediment and the extraction of reactive 10Be/9Be ratios, Chemical Geology, 318, 126-138, https://doi.org/10.1016/j.chemgeo.2012.04.031, 2012.

Western Regional Climate Center (WRCC): https://wrcc.dri.edu/, last access: 18 September 2020, 2005.

You, C. F., Lee, T., and Li, Y. H.: The partition of Be between soil and water. Chemical Geology, 77(2), 105-118, https://doi.org/10.1016/0009-2541(89)90136-8, 1989.

Figures

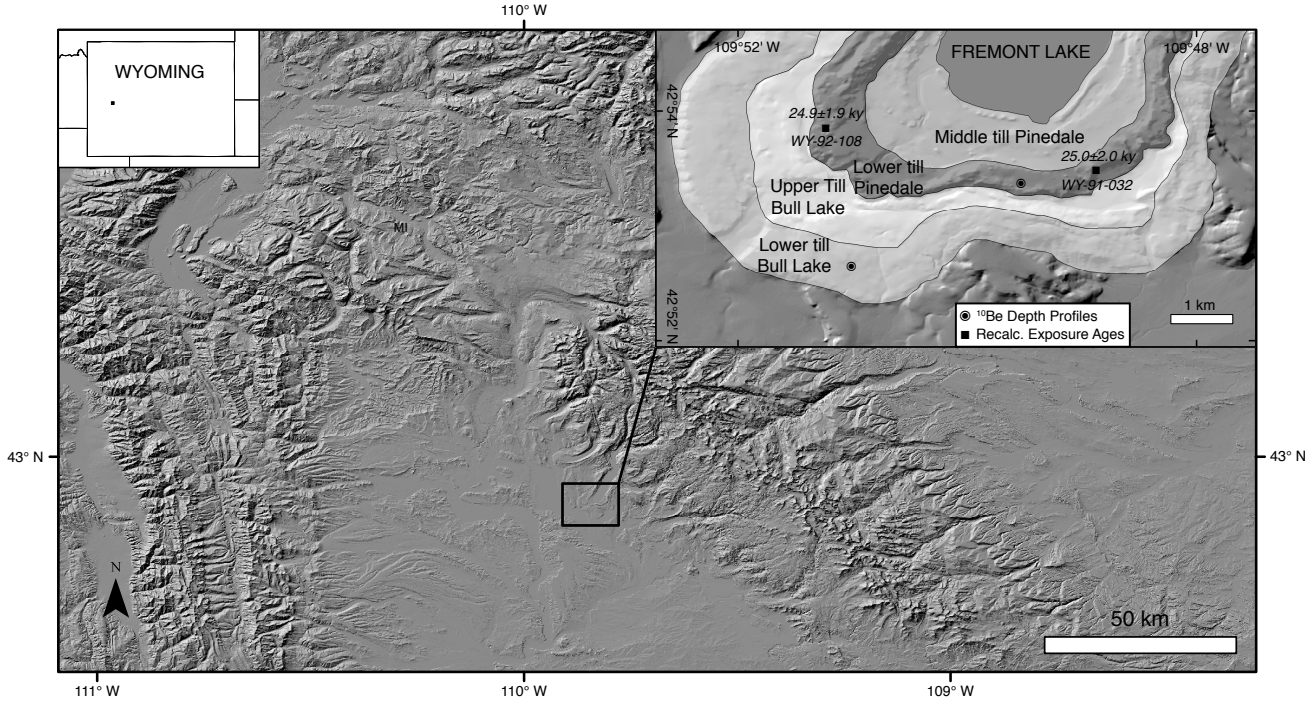

Fig. 1) Hillshade map of the Wind River range, derived from a 10 m digital elevation model (DEM); regional map encompasses the entirety of the meteoric ^{10}Be flux map grid cell of Heikkila and von Blanckenburg (2015). Inset (upper left) shows location of regional map within Wyoming. Inset (upper right) shows locations of depth profiles analyzed for cosmogenic nuclide concentrations from the terminal Pinedale and Bull Lake moraines in the Fremont Lake area (after Richmond [1973] and Schaller et al. [2009a]). Also shown are the locations of boulder surface exposure dates for the Pinedale moraine (WY-92-108 and WY-91-032 of Gosse et al., 1995) that were recalculated using revised parameters (Table S1) to establish an updated independent age constraint for this moraine.

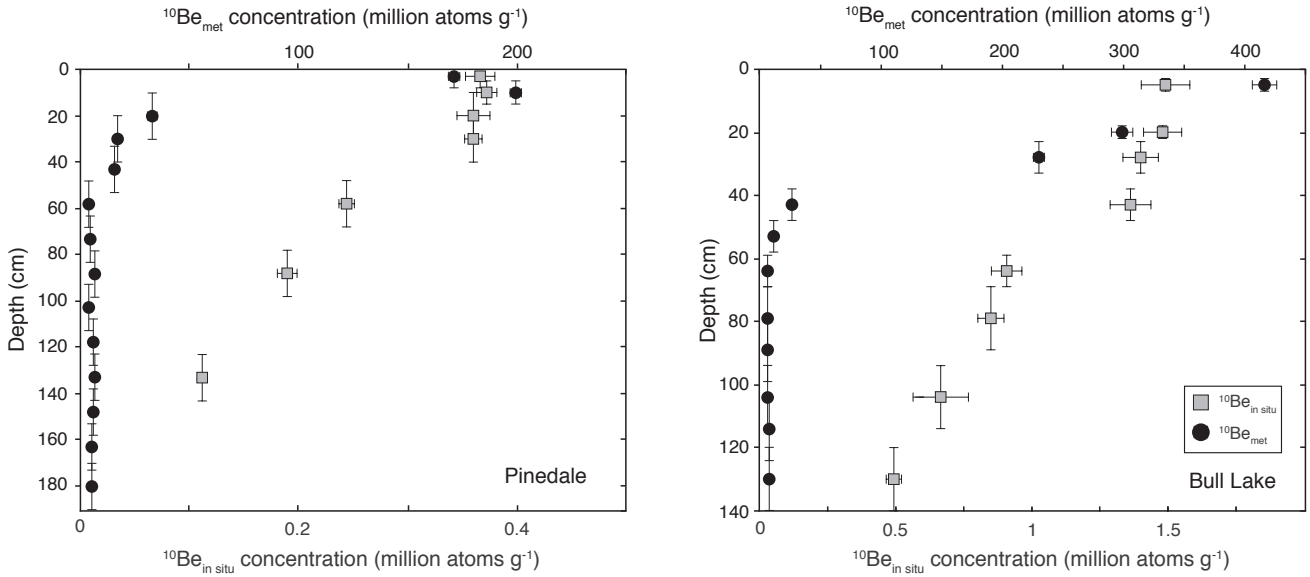

Fig. 2) (Left) Depth profile for the Pinedale moraine; $^{10}Be_{met}$ concentrations were measured from the <2 mm grain-size fraction of 14 samples from the same depth profile as analyzed for $^{10}Be_{in\ situ}$ in Schaller et al. (2009a). (Right) Depth profile for the Bull Lake moraine; $^{10}Be_{met}$ concentrations were also measured from the <2 mm grain-size fraction of 11 samples from the same depth profile as analyzed for $^{10}Be_{in\ situ}$ in Schaller et al. (2009a). The $^{10}Be_{met}$ concentration at 94 cm was not measured.

Table 1. ^{10}Be Concentrations and GSD[a] in Depth Profiles from Pinedale and Bull Lake Moraines

Sample[b]	Depth (cm)	Sand (wt %)	Silt (wt%)	Clay (wt %)	*In situ* ^{10}Be concentration[c] (10^5 atoms g^{-1})	Meteoric ^{10}Be sample weight (g)	^{9}Be carrier weight (mg)	Meteoric ^{10}Be concentration[c] (10^6 atoms g^{-1})	Meteoric ^{10}Be inventory (10^6 atoms cm^{-2})
Pinedale moraine (2262 m asl, 42° 53′ 26″ N, 109° 49′ 34″ W)									
04-WRMP-014	3 ± 2	75	18	6	3.67 ± 0.14	4.5747	0.2146	171.283 ± 5.142	1027 ± 30
04-WRMP-013	10 ± 5	68	22	10	3.73 ± 0.09	3.1697	0.2146	199.526 ± 5.986	2793 ± 84
04-WRMP-012	20 ± 10	70	23	7	3.60 ± 0.15	6.4287	0.2146	33.007 ± 3.183	660 ± 64
04-WRMP-011	30 ± 10	74	22	4	3.60 ± 0.08	6.1094	0.2148	16.819 ± 1.541	336 ± 31
04-WRMP-010	43 ± 10	76	19	5	-	5.1606	0.2144	15.357 ± 1.189	399 ± 31
04-WRMP-009	58 ± 10	82	15	3	2.44 ± 0.07	5.6470	0.2146	3.966 ± 0.336	119 ± 10
04-WRMP-008	73 ± 10	85	12	3	-	5.4438	0.2142	4.673 ± 0.382	140 ± 11

04-WRMP-007	88 ± 10	81	16	3	1.89 ± 0.09	5.6027	0.2140	6.699 ± 0.563	201 ± 17
04-WRMP-006	103 ± 10	82	15	3	-	6.0067	0.2103	3.569 ± 0.322	107 ± 10
04-WRMP-005	118 ± 10	71	23	6	-	3.0500	0.2127	6.207 ± 0.284	186 ± 9
04-WRMP-004	133 ± 10	71	24	5	1.11 ± 0.03	3.1070	0.2134	6.489 ± 0.302	195 ± 9
04-WRMP-003	148 ± 10	74	21	6	-	2.9340	0.2128	5.656 ± 0.249	170 ± 7
04-WRMP-002	163 ± 10	72	22	6	-	2.8869	0.2107	5.531 ± 0.240	166 ± 7
04-WRMP-001	180 ± 10	72	23	6	-	3.0824	0.2135	5.098 ± 0.236	173 ± 8
								∫	6672 ± 122
Bull Lake moraine (2285 m asl, 42° 52′ 39″ N, 109° 51′ 00″ W)									
AT-FL-4L	5 ± 2	69	22	9	14.9 ± 0.9	1.0174	0.4125	415.475 ± 12.464	4155 ± 125
AT-FL-4K	20 ± 5	51	29	20	14.8 ± 0.7	1.0793	0.2139	298.813 ± 8.965	8964 ± 269
AT-FL-4J	28 ± 5	52	34	14	14.0 ± 0.6	1.0824	0.2140	230.442 ± 6.913	3687 ± 111
AT-FL-4I	43 ± 5	47	23	30	12.3¤ ± 0.7	1.0593	0.1963	26.590 ± 0.798	798 ± 24
AT-FL-4H	53 ± 5	50	28	22	-	1.0176	0.2141	11.433 ± 0.343	229 ± 7
AT-FL-4G	64 ± 5	54	26	20	9.08 ± 0.56	1.0109	0.2144	7.083 ± 0.382	156 ± 8
AT-FL-4F	79 ± 10	60	24	16	8.50 ± 0.48	1.01	0.2141	6.639 ± 0.236	199 ± 7
AT-FL-4E	89 ± 10	62	24	14	-	1.0722	0.2142	6.318 ± 0.246	126 ± 5
AT-FL-4D	94 ± 10	75	17	9	-	-	-	6.723[d]	134[d]
AT-FL-4C	104 ± 10	64	26	10	5.98¤ ± 1.00	1.0164	0.2144	7.129 ± 0.428	143 ± 9
AT-FL-4B	114 ± 10	60	25	15	-	1.0283	0.2142	8.021 ± 0.241	160 ± 5
AT-FL-4A	130 ± 10	60	25	15	4.93 ± 0.28	1.0294	0.2143	8.449 ± 0.253	270 ± 8
								∫	19021 ± 318

[a]Grain size distributions and *in situ* ^{10}Be concentrations from *Schaller et al. (2009a)*

[b]See Schaller et al. (2009a) for the grain size fraction analyzed for each sample

[c]Corrected for blank, reported error includes analytical uncertainties (1σ)

[d]Average of $^{10}Be_{met}$ concentations from directly above and below this depth

¤Average of multiple aliquots analyzed in Schaller et al. (2009a)

Table 2. Recalculated Chi-Square Solutions for Different Denudation Rate Simulations of Schaller et al. (2009a)[a]

Type of Denudation	Model	Age (ky; *fixed parameter*)	Average Denudation (mm ky^{-1})	Inherited ^{10}Be concentration (10^5 at g^{-1})	Mixing Depth (cm)	Diffusivity *k* (10^{-3} m^2 y^{-1})	Maximum Height (m)	Slope Angle (degrees)
Pinedale moraine (2262 m asl, 42° 53′ 26″ N, 109° 49′ 34″ W)								
Constant	2	25	15	0.2	0			
Transient	4	25	29-35	0.2	0	20	30	25,30
Bull Lake moraine (2285 m asl, 42° 52′ 39″ N, 109° 51′ 00″ W)								
Constant	6	140	7.5	1.4	0			
Transient	8	140	6-21	1.2-1.8	0	0.3-10	35,40,50,60	5,10,15, 20,25,30

[a]For a full explanation of range allowed and resolution of each parameter, see Table 3 of *Schaller et al. (2009a)*

Table 3. $^{10}Be_{met}$ flux estimates, raw and normalized for Holocene paleointensity variations

Method	$F(^{10}Be_{met})$ uncorrected (x 10^6 atoms $cm^{-2}y^{-1}$)	Valid over time scale (ky)	$^{10}Be_{met}$ correction factor relative to Modern	$^{10}Be_{met}$ correction factor relative to Holocene	$F(^{10}Be_{met})$ corrected to represent Holocene (x 10^6 atoms $cm^{-2}y^{-1}$)	Transient Erosion Rate (g cm^{-2} y^{-1})[e]
Pinedale (This Study)	1.08 (+0.10/-0.16)	6	0.88[a]	0.71[a]	1.52 (+0.11/-0.21)	0.0064 (+0.0006/-0.0010)
Bull Lake (This Study)	1.05 (+0.35/-0.40)	24	0.99[a]	0.80[a]	1.28 (+0.43/-0.50)	0.0025 (+0.0009/-0.0010)
Graly et al. (2011)	0.55	0.005	0.82[b]	1.06[c]	0.83	-
Heikkilä and von Blanckenburg (2015)	-	10	1.23[c]	-	1.38 (+ 0.99)[d]	-

[a] *using measured $^{10}Be_{met}$ seafloor accumulation record of Christl et al. (2010) from 6 ky and 24 ky to present for the Pinedale and Bull Lake moraines, respectively*

[b] *using the paleomagnetic scaling method of Masarik and Beer (2009)*

[c] *using the paleomagnetic reconstruction method of Steinhilber et al. (2012)*

[d] *uncertainty represents the 'industrial' modeled flux of Heikkilä and von Blanckenburg (2015)*

[e] *calculated for a soil density of 2000 kg m^{-3}*